



UNIVERSITÀ
DEGLI STUDI
FIRENZE

FLORE

Repository istituzionale dell'Università degli Studi di Firenze

Chemisorption of nitronyl-nitroxide radicals on gold surface: An assessment of morphology, exchange interaction and decoherence

Questa è la versione Preprint (Submitted version) della seguente pubblicazione:

Original Citation:

Chemisorption of nitronyl-nitroxide radicals on gold surface: An assessment of morphology, exchange interaction and decoherence time / Poggini L.; Lunghi A.; Collauto A.; Barbon A.; Armelao L.; Magnani A.; Caneschi A.; Totti F.; Sorace L.; Mannini M.. - In: NANOSCALE. - ISSN 2040-3364. - STAMPA. - 13:(2021), pp. 7613-7621. [10.1039/d1nr00640a]

Availability:

The webpage <https://hdl.handle.net/2158/1242736> of the repository was last updated on 2021-09-10T13:26:59Z

Published version:

DOI: 10.1039/d1nr00640a

Terms of use:

Open Access

La pubblicazione è resa disponibile sotto le norme e i termini della licenza di deposito, secondo quanto stabilito dalla Policy per l'accesso aperto dell'Università degli Studi di Firenze (<https://www.sba.unifi.it/upload/policy-oa-2016-1.pdf>)

Publisher copyright claim:

La data sopra indicata si riferisce all'ultimo aggiornamento della scheda del Repository FloRe - The above-mentioned date refers to the last update of the record in the Institutional Repository FloRe

(Article begins on next page)

ARTICLE

Received 00th January 20xx,
Accepted 00th January 20xx

DOI: 10.1039/x0xx00000x

Chemisorption of nitronyl-nitroxide radicals on gold surface: an assessment of morphology, exchange interaction and decoherence time.

Lorenzo Poggini,^{a,b*} Alessandro Lunghi,^{a,‡} Alberto Collauto,^{c,†} Antonio Barbon,^c Lidia Armelao,^{c,d,e} Agnese Magnani,^f Andrea Caneschi,^g Federico Totti,^{a*} Lorenzo Sorace,^{a,*} Matteo Mannini^a

A combined ToF-SIMS, XPS and STM characterization has been adopted here to study the deposition of a sulphur-functionalized nitronyl nitroxide radical on Au(111) clearly demonstrating the chemisorption of intact molecules. EPR characterization showed that the radical molecules maintain their paramagnetic character. Pulsed EPR measurements allowed to determine the decoherence time of the nanostructure at 80 K, which turned out to be comparable to the one measured in frozen solution and longer than previously reported for many radicals and other paramagnetic molecules at much lower temperatures. Furthermore, a state-of-the-art *ab initio* molecular dynamics study has been performed, suggesting different possible scenarios for chemisorption geometries predicting the energetically favoured geometry. The calculated magnetic properties indicate a partial non-innocent role of the gold surface in determining the magnetic interactions between radicals in packed structures. This suggests that the observed EPR spectrum is to be attributed to low-density domains of disordered radicals interacting via dipolar interactions.

Introduction

Monolayers of magnetic molecules are attracting broad interest thanks to their potential technological applications as building block units in new devices for molecular spintronics¹ and quantum computation.^{2,3} A crucial step in this direction is the control of the deposition of magnetic material forming a single layer. Self-assembling of monolayer (SAM)⁴ is one of the most used techniques to achieve a bidimensional array of (quasi-)ordered molecules absorbed on the surface from

diluted solution. Prerequisite of the SAMs formation is the introduction of functional groups allowing specific (covalent) interactions with a given surface. A 2D regular structure can then be obtained by optimizing intermolecular interactions between nearest neighbours.⁴ This strategy can be extended to molecules featuring specific functionalities, such as magnetic or optical properties. In the case of polynuclear clusters behaving as Single-Molecule Magnets (SMM),⁵ previous studies showed that this fine control is only partially achievable due to their steric hindrance and to their multiple grafting arrangements,^{6–8} while it has been successfully employed for organic radicals.^{9–16} During the last decade different approaches were used to deposit pure organic radical molecules on surfaces using either High Vacuum (HV) / Ultra High Vacuum (UHV)^{16–22} approaches or wet chemistry (i.e. Langmuir-Blodgett and SAM).^{9,13,23} However, to date, only a few of papers have tackled the adsorption of the pure organic radicals at the computational level.²⁴

The interest toward nitronyl-nitroxide radicals (**Nit**) germinated from the observation of long-range magnetic order at low temperature in bulk phases²⁵ and from the possibility of using them as building blocks of more complex magnetic structures such as Single-Chain Magnets.^{26–28} Nowadays the key interest for potential magneto-transport and quantum computation purposes is related to the spin dynamic properties of **Nits**: they features relatively long spin-lattice (T_1) and significant decoherence (T_2 or T_m) times in frozen solutions at a temperature as high as liquid nitrogen and without the need of

^a Department of Chemistry "Ugo Schiff" and INSTM Research Unit, University of Florence, I-50019 Sesto Fiorentino, Italy. E-mail: lorenzo.sorace@unifi.it

^b ICCOM-CNR, via Madonna del Piano 10, 50019 Sesto, Fiorentino, Italy. E-mail: lpoggini@iccom.cnr.it

^c Department of Chemical Sciences and INSTM Research Unit, University of Padova, I-35131 Padova, Italy

^d Institute of Condensed Matter Chemistry and Technologies for Energy, National Research Council of Italy, ICMATE-CNR, via Marzolo 1, 35131 Padova, Italy

^e Department of Chemical Sciences and Materials Technologies, National Research Council of Italy, DSCTM - CNR, Piazzale A. Moro 7, 00185 Rome, Italy

^f Department of Biotechnologies, Chemistry and Pharmacy, and INSTM Research Unit, University of Siena, I-53100 Siena, Italy

^g DIF – Department of Industrial Engineering and INSTM Research Unit, University of Florence, Via S. Marta 3, I-50139 Florence, Italy

[†] Present address: Goethe-Universität Frankfurt am Main

^{*} Present address: School of Physics, CRANN Institute, AMBER centre, Trinity College, Dublin 2, Ireland

Electronic Supplementary Information (ESI) available: Experimental section; computational details; Additional XPS data and analysis; ToF-SIMS data and analysis; STM images; Additional EPR data and computation results, as figures and tables. See DOI: 10.1039/x0xx00000x

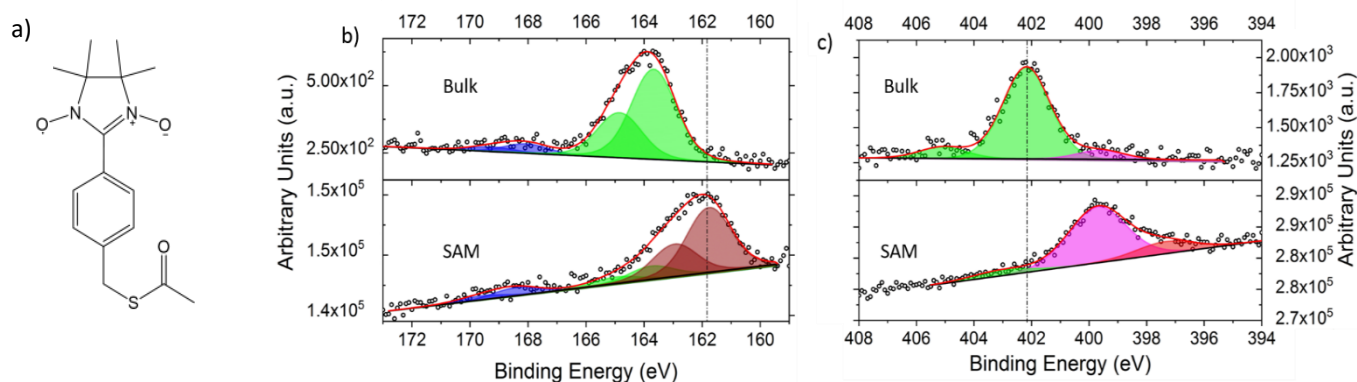


Figure 1. a) Chemical structure of thio-acetic acid 4-(nitronyl-nitroxide radical)benzyl ester, **1**; XPS spectra of **1** in the S2p region (b) and in the N1s region (c) in bulk (drop cast) and on surface evidencing the contributions from the different spectral components required for least squares fitting. In (b) green curves correspond to R-S-Ac component, while brown ones to R-S-Au component of the S2p signal. In (c) green curves correspond to R-NO N1s component while pink ones to R-N-H N1s component.

using deuterated or proton-free solvents.²⁹ Thanks to these properties and their inherent quantum nature, they have also been proposed, together with other radical families, as potential molecular-based qubits, or as elements of spintronics devices.^{30–36} Indeed, recent works suggest that **Nit** function can be used to influence the spin injecting electrode in hybrid vertical spin valves.³⁴ In this perspective, the investigation of the decoherence properties of organic radicals organized in addressable arrays on surfaces is a key point in the quest for technological use of these systems. However, to the best of our knowledge, this issue has not been addressed yet. We aim to move a step forward in this direction by reporting here a complete characterization of a SAM of a sulphur-functionalized **Nit**, the thioacetic acid 4-(nitronyl-nitroxide radical)benzyl ester (**1**, Figure 1a), on Au(111) including a first attempt of evaluating the spin relaxation properties of this monolayer. A complete description of the system is obtained by combining time-of-flight secondary ion mass spectrometry (ToF-SIMS) and X-ray Photoelectron Spectroscopy (XPS) to provide the chemical characterization of the chemisorbed monolayer and room temperature scanning tunnelling microscopy (STM) to achieve a morphological characterization of the deposit. The characterization of the static and dynamic magnetic properties of the nanostructured radical has been achieved by continuous-wave (cw) and pulsed electron paramagnetic resonance (EPR) spectroscopy. This set of experiments has been flanked by a state-of-art theoretical investigation as ab initio molecular dynamics (AIMD) to get further insights about the favoured chemisorption configuration and static DFT approach for the calculations of intermolecular magnetic interactions in the SAM.

Results

SAM preparation and chemical characterization

The synthetic strategy adopted to introduce the thioacetic group needed to promote the chemisorption of the **Nit** moiety on gold has been described elsewhere.³⁷ Here we focused on the characterization of the SAMs of **1**, which were prepared by

incubating a hydrogen-flame annealed slab of gold^{9,38} in a 3 mM solution of **1** in dichloromethane under reflux condition for 24 hours in the dark.⁹ After the incubation procedure the spontaneous and quantitative (75%) removal of the thioacetyl protection and the formation of a chemical bond between the sulphur of the linker group and the gold surface has been confirmed by using in-house XPS analysis (see Figure 1 and Table S1). The XPS spectra of the SAM sample show the presence of clearly detectable intense peak in the S2p_{3/2} region at 161.8 eV, a binding energy (BE) that is lower than the one found in the bulk sample obtained by drop-cast (163.7 eV) (see Figure 1b). The ratio and BE difference between components S2p_{3/2} and S2p_{1/2} is maintained in passing from the bulk (drop cast) to the chemisorbed sample. The further presence of spectral features at 163.7 eV and 168.4 eV points to a small number of physisorbed molecules (less than 16%) and minimal oxidation of the linking group (14%) that significantly support the compactness of the obtained monolayer.^{39,40} As for the N1s region, XPS spectra of both the bulk phase and the SAM evidence the onset of an X-ray induced photoreduction process occurring at the nitrogen. Indeed, in addition to the principal component at 403.6 eV (Figure 1c) which is typical for **Nit** systems¹⁸, another component at 399.7 eV is observed in the bulk of **1**, the intensity of which increases on increasing X-ray exposure (see Figure S1). The peak has been attributed to nitrogen atoms in N-H group forming upon photoreduction. Beside this, we point out the presence of a weak additional contribution at 397.5 eV, which supports the presence of a small fraction of molecules (ca. 8%) in which nitrogen atoms are involved in a direct Au-N bond.¹⁷ Within the error limits, the semi-quantitative analysis obtained by integrating the whole S2p and the N1s XPS signals, reveals a good agreement of the N/S ratio with the theoretical expectations (2.0) both for the bulk sample obtained by drop-casting on gold (1.9) and for the SAM (1.6) (see Table S1 and XPS experimental details in Supplementary Material). This result supports the hypothesis that chemisorption does not alter the molecular framework. ToF-SIMS⁴¹ characterization of the SAM further confirms the occurrence of chemisorption of the intact system, showing some relevant signals not detected in the bulk material at 505.3

m/z , 461.3 m/z , 447.3 m/z and 445.3 m/z : according to our analysis (see Figure S2 in ESI and Table S2) these can be attributed to a gold atom directly interacting with the sulphur atom of the molecular backbone. In particular, the isotopic pattern centred at 461.3 m/z (Figure S2d) can be correlated to a $[M-O-Ac+2H+Au]^+$ fragment, observable only in SAM sample due to the chemical grafting with Au. The assignments for the lower m/z peaks (247.1 - 323.1 m/z) reported in Table S2 both for SAM and the bulk, are obtained by considering the simultaneous loss of oxygen atoms from the nitroxide function followed by the typical rearrangement observed in other Nit bulk system.⁹ The formation of a single layer deposit is further corroborated by the room temperature STM characterization we reported in Figure S3: indeed, this experiment in air, reveals the presence of the typical defects of SAMs (pinholes)⁴² thus excluding the formation of multi-layered structure. Thanks to those characterization we can assume that the chemical structure and the stoichiometry are retained after the wet chemistry deposition process.

EPR spectroscopy

EPR spectroscopy (see ESI for Experimental details) has been used as a key tool for the characterization of the magnetic properties of the monolayer of **1**. The room-temperature cw-EPR spectrum (Figure 2) of the SAM of **1** is similar to the one reported for other nitronyl-nitroxide derivatives assembled on gold,^{9,11} with clear evidence of the hyperfine pattern due to the coupling of the unpaired electron with the two equivalent ^{14}N ($I=1$) nuclei. The observation of a spectrum with resolved hyperfine features close to those of **1** in toluene solution testifies that the paramagnetic character is preserved after chemisorption and further confirms that the process occurs by maintaining the integrity of the Nit function (i.e. without degradation to the corresponding imino-nitroxide). A qualitative analysis of the cw-EPR spectra of the SAM of **1** at different temperatures (Figure 2a) evidences a narrowing of the homogeneous linewidth on increasing temperature. The relatively narrow, powder-like, lines observed at room temperature, indicate that the dynamics in this temperature range fall into a fast motion regime with restricted width. This hypothesis is also in line with the relatively easy saturation, which can be observed already at 20 dB (Figure S4). In agreement with such a fast dynamics and the consequent absence of any long-range geometric order, no angular dependence of the EPR spectrum has been observed at room temperature (Figure S5). Moreover, the observed spectral pattern at 294 K is rather similar to the one observed in frozen toluene solution at 80 K, but with a reduction of the total width by ca. 0.5 mT. This observation is the main evidence of a restricted mobility, faster at higher temperatures, which leads to a partial averaging of the z-component of the hyperfine interaction. From the reduction of the spectral width, we estimate an amplitude of ca 17°.⁴³ Because of internal constraints, the major contribution of the motion is likely a twist around the phenyl C1-C4 axis, but a twist around the carbon-sulphur σ -bond can also contribute (see further). These

rotational/librational degrees of freedom of radicals are consistent, at high temperature, with a full isotropization of the EPR spectrum, and support the hypothesis of a low-density packing of **1** on the Au surface. Furthermore, the large line broadening, well visible at 80 K, indicates a slowdown of the motion and the onset of splitting from electron-electron interactions (see below).

In order to study both the dynamics and the spin-spin interaction, we attempted to record echo-detected EPR (EDEPR) spectra for the SAM of **1** close to liquid nitrogen temperature. Despite the small amount of sample ($< 10^{14}$ spins) we were able to observe a definite spectrum after 12 h acquisition (Figure 3, a and c). This is the first important indication that the decoherence time for a consistent part of the

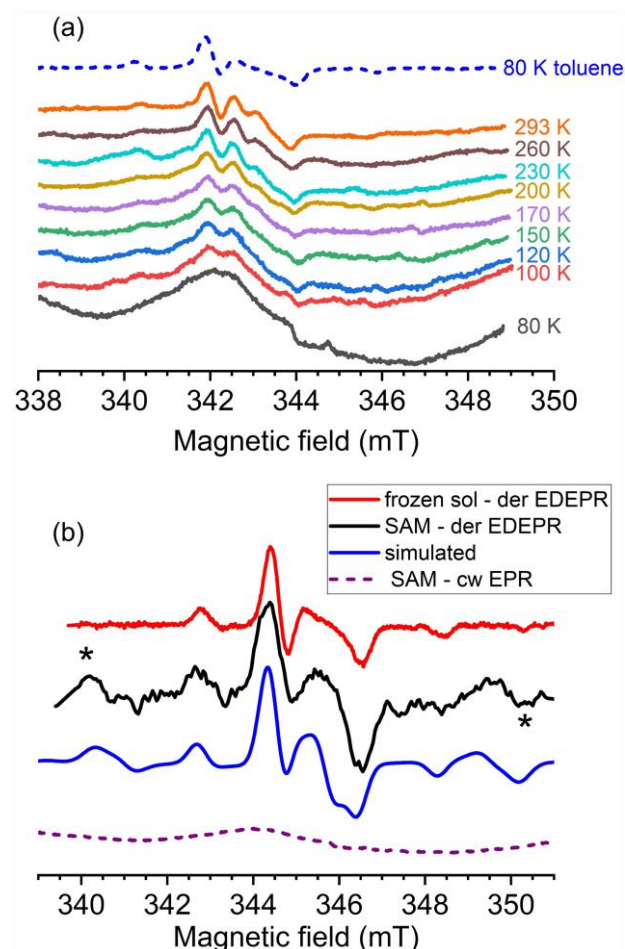


Figure 2. (a) Temperature dependence of the X-band cw-EPR spectrum of a SAM of **1**. The cw-EPR of **1** in toluene at 80 K is reported for reference. (b) Comparison of the derivative Echo detected spectra at 80 K and $\tau = 200$ ns for SAM sample (black) and for the toluene solution (red). The asterisks highlight the extra bands present in the SAM sample. In blue the simulation of the SAM sample (reported in Table S3) by using parameters close to those obtained for the thio-acetic acid 4-(nitronyl-nitroxide radical)benzyl ester in toluene frozen solution³¹. The simulation of the side bands is relative to a pair of radicals with a dipolar interaction of $|D| = 510$ MHz with the largest direction of interaction approximately along the Z-component of the ^{14}N tensor, by supposing that they stack face-to-face. For comparison, the cw-EPR of the SAM sample at the same temperature is given (dashed line).

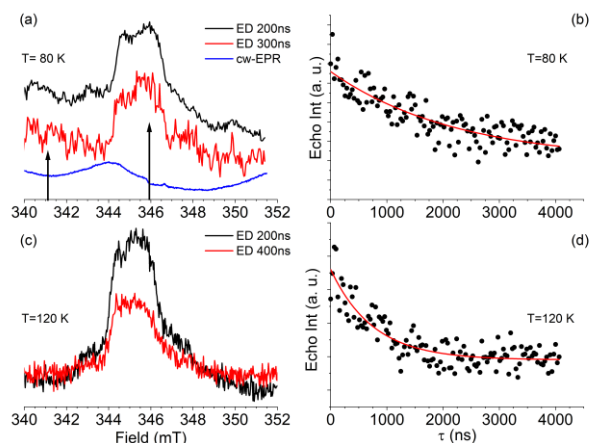


Figure 3. Echo detected EPR spectra (left) of a SAM of **1**, acquired with different delay times at 80 K (a) and 120 K (c). Corresponding Hahn echo decays as obtained from on-resonance conditions minus off-resonance conditions (see arrows) at the same temperatures are reported in panel (b) and (d).

sample is long, and therefore, the detection of a measurable echo was possible.

The lineshape of the derivative of the echo-detected spectrum of the SAM of **1** at 80 K is rather similar to that of **1** obtained in frozen toluene (Figure 2b),²⁹ but different with respect to the cw-EPR spectrum of **1** in the SAM at low temperature. These observations point to the formation of SAM domains of **1** with different mobility of the radical and/or different spin-spin interaction. Radicals with low mobility and small spin-spin interactions result in domains where the molecules are isolated, having a residual librational motion larger than in toluene, and which accounts for the slightly larger linewidth.

In the EDEPR spectrum (Figure 2b), we note the clear presence of narrow sidebands, indicating a definite spin-spin interaction. These bands could be reproduced in the simulation⁴⁴ by assuming that the spectrum is a superposition of different contributions: isolated (the majority) and mildly interacting spins (dipolar interaction). The best reproduction of the spectra was obtained by assuming $|D|=510$ MHz, (corresponding to a distance of ca. 5.3 Å along the nitrogen p_z -axes (see Table S3 for best simulation parameters).

To determine the decoherence time T_m of these samples, Hahn echo decay curves (Figure 3b and d) were measured at 80 K and 120 K (Figure 3c and d) by removal of the off-resonance decay signal from the on-resonance one. These curves were fitted to the expression:

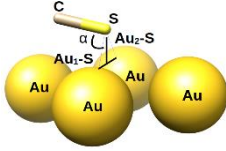
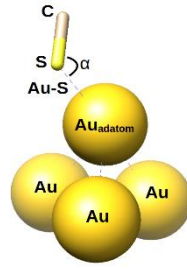
$$I(2\tau) = I_0 + A_f \exp(-2\tau/T_{m,f}) + A_s \exp(-2\tau/T_{m,s}) \quad (1)$$

where τ is the inter-pulse delay time, A_f and A_m account for the relative contributions of the fast and slow components and $T_{m,f}$, $T_{m,s}$ are the corresponding decay times. The first component, with low weight, is attributed to a non-perfect subtraction of the off-resonance signal, while the second one is the actual relaxation of the radical SAM. At 80 K, the best fit parameters were $T_{m,f} = 0.2 \pm 0.2$ μ s and $T_{m,s} = 5 \pm 1$ μ s with a relative weight of $A_f = 1.0$ and $A_s = 0.3$. At 120 K the fast component (background) signal is strongly reduced and the lineshape of the

EDEPR is slightly different. Fit of the Hahn decay gave a phase memory time of $T_m = 1.5 \pm 0.2$ μ s.

On the other hand, cw-EPR spectra at low temperature shows, superimposed to the signals of the domains determined by spin-echo methods, a broad and almost featureless band. In order not to be detected by EDEPR the relaxation times of the species responsible for this signal must be fast. Two possible reasons can be invoked for a shortening of the relaxation times: a slow-motion regime that induce a broadening of the lines or the onset of exchange interactions.

Computational results

Cell	Position	Au _{1,2} -S Å	Au _{1,2} -S-C α , °
 1@Au_{clean,up}	bridge	2.55(3) 2.71(7)	101.8(2) 121(5)
 1@Au_{recon,up}	atop	2.33(1)	106.4(2)

^a Values in parenthesis are presented to show the differences within two geometrical "equivalent" adsorption pairs in Au_{clean}.

^b Values in parenthesis are presented to show the differences within two geometrical "equivalent" adsorption pairs Au_{recon}.

Table 1. Calculated geometrical parameters of **1** adsorption after optimization: the schematic representation of the Nit molecule is limited to the Carbon and Sulphur atoms for clarity sake

A computational study was undertaken to get a more detailed comprehension of the structure and morphology of the radical chemisorbed on surfaces, as well as to pave the way for further theoretical and experimental investigations focused on the dynamic properties of this system. The chosen approach is based on the ones reported elsewhere.^{6–8,45,46} Two different model substrates were considered, namely an unreconstructed (**Au_{clean}**) and reconstructed (**Au_{recon}**, see ESI for computational details) gold surfaces. For both surfaces, calculations point to a high symmetry arrangement of the radicals, the two differing in the binding modes for the sulphur atoms: in a bridge position for radicals on **Au_{clean}** (**1@Au_{clean}** hereafter) and atop the

adatoms for radicals on **Au_{recon}** (**1@Au_{recon}** hereafter), see Table 1.

Both scenarios resulted in a regular and almost identical hexagonal pattern, with the radicals laying orthogonal to the surface.

This suggests that any reconstruction of the surface would not significantly affect the symmetry and the geometrical parameters of the unit cell of the adsorbed radicals.

To check for this point, the time evolution of the functionalized surface was calculated by AIMD for both cases. In the **1@Au_{clean}** scenario, all the radicals start relaxing from their stand-up positions (**1@Au_{clean,up}** from now on) to a laid-down conformation (**1@Au_{clean,down}** from now on), which is maintained to the end of the thermalization stage and for all the following simulation time (see Figure S6).

Interestingly, each radical adheres to the surface along the same direction, leading to an almost regular pattern of their NO groups. This conformation (**1@Au_{clean,down}**) gives an enthalpic gain of 27.7 kcal/mol with respect to the starting one and suggests that at this level of coverage dispersive forces and π - π interactions are not efficient enough to make an upstanding conformation likely.

For **1@Au_{clean,down}**, the AIMD run evidences a distribution of the gold surface-nitroxide (Au-(N)O) distances in the range of ~ 1 Å to ~ 7 Å, with two maximal probability values of 2.2 and 4.2 Å (see ESI Figure S7). At these distances the π^* orbital of NOs groups is expected to directly overlap with the gold surface electron density, with a consequent possible transfer of the unpaired electron to the reservoir of gold electronic bands. The two inequivalent NOs groups are lying between ~ 3 Å and ~ 7 Å from the gold surface, which is consistent with what has been found in similar system.^{9,46} Denser coverages have been tested but they led to decomposition of at least one Nit. These results suggest that the steric hindrance of nitronyl-nitroxide groups cannot be compensated by attractive dispersion forces. This is further confirmed by the distribution of the binding sulphur atoms with respect to the gold atoms of the first layer (Figure 4) and by the analysis of sulphur atoms coordination numbers spanned throughout the AIMD (Figure S8). The results reported in Figure 4 further indicate that the sulphur atoms mobility is quite low with no evidence of diffusion. Indeed, the grafting S sites are localized with a range of S-S distances of 8.3-9.3 Å

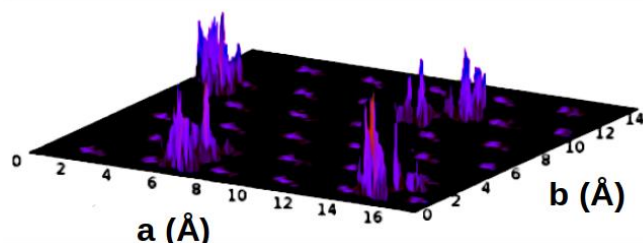


Figure 4. Probability of finding Sulphur atoms on the gold surface. Darker colours are associated to low probability (lower peaks) while brighter ones to high probability (higher peaks). Small smooth spots in the hexagonal pattern represent the possible positions of the Gold atoms of the first layer for which the probability

has been removed for sake of clarity. The dimensions of a and b are the ones of the simulation cell (see ESI).

As for the **1@Au_{recon}** scenario, the AIMD runs show a prompt change of the local geometry of the Au-S. Indeed, the sulphur atoms move from atop the gold adatom to a staple position (see Figure S9). Immediately after, as already observed for the **1@Au_{clean}** case, a relaxation of the radicals from an upstanding conformation to a laid down one was calculated. A large enthalpic gain of 30.02 kcal/mol was observed also in this case. At variance with **1@Au_{clean}**, the NOs groups did not arrange in an ordered pattern and gave a larger number of different quasi-degenerate conformations. However, it is likely that a higher order might be eventually reached by increasing the time used to study the conformational space. Interestingly, in this new structure (**1@Au_{recon,down}** hereafter), we observe an oxygen atom of a NO group directly interacting with an adatom ($O_{\text{adatom}} = 2.41$ Å, see Figure S9b).

Therefore, AIMD indicates that **1@Au_{clean,down}** and **1@Au_{recon,down}** represent the most likely scenarios mimicking experimental highly packed SAMs if the thermodynamic data are considered. This is in contrast with previous reports on other Nit^{45,46} and different organic radical based SAM⁴⁷, where the temperature effects are not taken into considerations. In this regard, these results are of great importance since indicate the necessity to take them into consideration to properly describe the grafting process when a system with a great structural mobility is considered.

Table 2. Computed spin density values (a.u.) for a single Nit radical with different bonding configurations for a gold clean surface: standing configuration (**1@Au_{clean,up}**), and lying down configuration, with single Nit oriented either parallel **1@Au_{clean,down,L}** or orthogonal to the surface **1@Au_{clean,down,I}**. **1_{isol}** is the radical in vacuum.

Atom	1_{isol}	1@Au_{clean,up}	1@Au_{clean,down,L}	1@Au_{clean,down,I}
O1	0.33	0.28	0.25	0.26
O2	0.33	0.28	0.32	0.27
N1	0.26	0.22	0.23	0.21
N2	0.26	0.22	0.22	0.21
Cα^a	-0.16	-0.13	-0.15	-0.13
Total	1.03	0.88	0.87	0.82

^a α -carbon atom of the nitronyl-nitroxide group.

Theoretical investigations may also provide useful information for the analysis of the magnetic properties of the SAM. As a first step, we calculated the spin density for different optimized structures obtained from different anchoring scenarios of a single Nit radical suggested by AIMD as guess geometries (Figure S9). Unreconstructed gold surface was considered as reference (Table 2, see ESI for details). It is worth to stress that the single molecule optimizations can be also considered as mimicking the low-density scenario vs. the closed packed one represented by the AIMD unit cells. Overall, a reduction of the spin density for both N and O ($< 25\%$) with respect to that of the isolated molecules is observed for all scenarios. This result indicates that the gold surface plays a role in the modulation of the magnetic properties of the single Nit. However, the presence of a direct overlap of the π^* orbitals with the gold

conductive bands does not significantly quench the paramagnetic character of the Nit radical. This is particularly evident for lying down radical configuration, with single Nit oriented orthogonal to the surface (**1@Au_{clean,down,L}**), showing a larger quenching (0.07 a.u.) for the oxygen atom closest to the surface (O1), while for the non-interacting one (O2) a decrease of only 0.01 a.u. is observed. These results are of much relevance since they support the EPR evidence of the persistence of the radical species upon adsorption and prompted us to simulate the STM images for the four conformations at 0.65 V (empty states).

In all the four scenarios, a hexagonal unit cell A x B was computed, with features which qualitatively agree with the experimental ones (see ESI, text, Figure S10 and Table S4), thus not allowing to draw definite conclusions.

With the aim of obtaining clearer indications on the preferred configurations, we theoretically investigated the possibility of exchange coupling magnetic interactions among the Nit radicals. Different exchange couplings were computed for the four possible conformations, leading to different ground states (see Table 3). The calculated magnetic interactions among the nitroxide centres in both **1@Au_{clean,up}** and **1@Au_{recon,up}** scenarios are very small, of the orders of few 10^{-2} cm^{-1} (comparable with the SCF convergence criterium). On the other hand, **1@Au_{clean,down}** and **1@Au_{recon,down}** scenarios show much larger magnetic interactions of the order of $1\text{--}2 \text{ cm}^{-1}$. This indicates that the surface plays a role in the propagation of the magnetic information among the radical centres and it is thus non-innocent. This is supported by the independence of J 's from the radical-radical distance, which indicates that direct overlap among the NO groups cannot be considered responsible for the calculated interactions. Spin densities plots for all the scenarios show a delocalization in the gold surface supporting its non-innocent role as super-exchange bus (Figure S11). Further proves of its active role is witnessed by the results obtained for model systems where the gold surface is removed (identified as **1@Au_{clean,down}** and **1@Au_{clean,up}** hereafter). In the case of the lying down conformation, the magnitude of the exchange interactions drops of almost two orders of magnitude when the gold surface is not included (see Table 3). It is worth to mention that the computed J for laid down configurations, where a super-exchange pathway via gold surface is established, are somehow biased by in their magnitude by the use of pure DFT (antiferro-magnetic contributions over-estimated). It is also evident that the inclusion of the dispersion forces corrections was determinant in getting more reliable geometries with respect to the ones found in ⁴⁵. Indeed, the computed J for the standing up scenarios are found similar in magnitude to the ones found in crystals for similar compound. ⁴⁸

Table 3. Computed exchange couplings (cm^{-1}) and ground states for the four possible configurations of radicals on gold surfaces and the two scenarios where gold surface has been removed (**1@Au_{clean,up}** and **1@Au_{clean,down}**) computed with PBE functional. In parenthesis, the values computed with B3LYP functional (see ESI for more details).

	J_1	J_2	J_3	J_4	GS
1@Au_{clean,up}	-0.08 (-0.21)	-0.04 (0.07)	-0.08 (-0.10)	-0.05 (0.03)	

1@Au_{clean,down}	-0.18 (-0.39)	0.26 (0.19)	0.14 (0.07)	0.29 (0.08)	
1@Au_{clean,up}	-0.06	-0.03	-0.08	-0.05	S=2
1@Au_{clean,down}	3.22	-6.93	-0.38	7.41	S=1
1@Au_{recon,up}	-0.05	-0.04	-0.09	-0.03	S=2
1@Au_{recon,down}	6.24	-6.57	-1.60	5.12	S=0

Discussion

The experimental characterization of the SAM of **1** showed unequivocally that it is safely chemisorbed on gold surface. The EPR results and the theoretical calculations allow to conclude that formation of the SAM occurs maintaining the paramagnetic character of the molecule and that the deposited molecules are characterized by fast dynamics (in the EPR timescale) and a restricted motion within cones of about 20 deg. Indeed, at high temperature, we observe an EPR spectrum which is quite close to that of the frozen solution. The spectrum is attributed to radicals with restricted mobility in fast motion regime, and, because of the relatively large adsorption enthalpy (of the order of 30 kcal/mol), likely the motion is a twist of the Nit group along its axis over the surface. Such motion can explain the reduction of the $^{14}\text{N } A_{zz}$ components.

From the thermodynamic point of view the most favourable calculated scenarios are those for which the radicals lay down on the surfaces, driven by the interaction of the phenyl and NO groups with the gold surface. DFT calculations also point to a non-innocent role of the surface, which transmits a relevant intermolecular exchange interaction between radicals, dependent on the absorption configuration. This is consistent with the observation of the Kondo effect in the weak coupling regime⁴⁹ for a different nitronyl-nitroxide radical on Au(111) where the magnetic impurities could be injected directly by the Nit itself through the homolytic break of the -S-Ac in the conduction bands as already suggested previously.^{45,46,50,51} Therefore, a magnetic interaction between impurities leading to magnetic ordering may arise ⁵² if the spin correlation generated by the radical-conduction electrons is preserved by the electrons which then interact with the other radical. This interaction is therefore expected to be strongly dependent on the temperature, if thermal relaxation processes can interfere in the transfer of the spin correlation. Therefore, the DFT magnetic calculations accounts for a low-temperature J value. The interaction with the surface, while of fundamental importance to transmit the exchange interaction, does not appear however to be large enough to quench the paramagnetic properties of the radical contrarily to what reported previously by different authors^{53,54} On the other hand, the strength of exchange coupling, while depending on the absorption configuration, is always calculated to be much larger than the hyperfine coupling to the nitrogen nuclei. Thus, for a compact monolayer of radicals an EPR spectrum much different from that of an isolated one would be expected. A single exchange-narrowed, dipolar broadened line has been indeed reported by different groups.^{47,55,56} For those systems, however, the standing conformation was suggested to be the

favoured one due to the structural features of the radicals. No temperature effects were taken into consideration though. Consequently, the exchange interaction was of the direct type and not mediated by the surface.

In the case of the SAM of **1**, exchange interactions are not visible at room temperature because of the relatively large mobility, able to average direct interaction, and because of the temperature, which quenches the interaction with the surface. The disorder in the orientation of Nit radicals is further supported by the absence of measurable angular dependence. At lower temperature EPR spectra evidence the presence of different domains. One is made up by slow relaxing radicals, observed by EDEPR; this suggests that they are located in environments that disfavour exchange interactions, i.e. in low-density packing regions. For some of these the dipolar pairwise interaction is visible. The second domain is evidenced by the broad featureless band in CW EPR, which are attributed to the tightly packed regions with non-negligible exchange interactions, as suggested by calculations.

The combination of calculations and spectroscopy then allows us to draw a very precise picture of the structure and properties of the sample. This is of particular interest since the isolated radicals maintain their long decoherence time, as observed by pulsed EPR. At 80 K the measured T_m is indeed comparable to the one measured in frozen solution²⁹ and longer than previously reported for many radicals and other paramagnetic molecules at much lower temperatures⁵⁷ and of the same order of magnitude of the Blatter radical in frozen solution.²⁰ While this is an important step toward the use of these systems in potential spintronics or QC devices, its attribution to disordered, low density packed radicals, suggests that future efforts must be aimed at obtaining an improved 2D order of the deposited radical, possibly on more innocent surfaces.

Summary and conclusions

Tof-SIMS, XPS and STM demonstrated that the thioacetic 4-(nitronyl-nitroxide radical)benzyl ester on Au(111) forms a SAM of intact molecules. EPR spectroscopy provided clear evidence of the persistence of the radical character of the molecules upon chemisorption, a result confirmed by state-of-art computational approach. The latter allowed to investigate different absorption scenarios in presence of clean and reconstructed surface and evidenced a partial delocalization of the radical spin density on the surface. This results in a non-innocent role of the surface, which is effective in transmitting intermolecular exchange interactions and potentially establish a Kondo effect. These interactions are not visible at high temperature.

Finally, we report the determination of decoherence time for nanostructured organic radical, showing that it maintains some promise for application in molecular spintronics.

Conflicts of interest

There are no conflicts to declare.

Acknowledgements

We acknowledge the European COST Action CA15128 MOLSPIN, the Quanterra ERA-NET Co-fund project SUMO and the FET Open Femtotera byte project for financial support. Italian MIUR, through PRIN project QCNaMoS (2015-HYFSRT) and Progetto Dipartimenti di Eccellenza 2018-2022 (ref. no. B96C1700020008), and Fondazione Ente Cassa di Risparmio di Firenze are also acknowledged for financial support

Notes and references

- 1 L. Bogani and W. Wernsdorfer, *Nat. Mater.*, 2008, **7**, 179–86.
- 2 M. Atzori and R. Sessoli, *J. Am. Chem. Soc.*, 2019, **141**, 11339–11352
- 3 G. Serrano, L. Poggini, M. Briganti, A. L. Sorrentino, G. Cucinotta, L. Malavolti, B. Cortigiani, E. Otero, P. Saintavit, S. Loth, F. Parenti, A. L. Barra, A. Vindigni, A. Cornia, F. Totti, M. Mannini and R. Sessoli, *Nat. Mater.*, 2020, **19**, 546–551.
- 4 A. Ulman, *Chem. Rev.*, 1996, **96**, 1533–1554.
- 5 D. Gatteschi, R. Sessoli and J. Villain, *Molecular Nanomagnets*, Oxford University Press, 2006
- 6 V. Lanzilotto, L. Malavolti, S. Ninova, I. Cimatti, L. Poggini, B. Cortigiani, M. Mannini, F. Totti, A. Cornia and R. Sessoli, *Chem. Mater.*, 2016, **28**, 7693–7702.
- 7 G. Fernandez Garcia, A. Lunghi, F. Totti and R. Sessoli, *Nanoscale*, 2018, **10**, 4096–4104.
- 8 L. Gragnaniello, F. Paschke, P. Erler, P. Schmitt, N. Barth, S. Simon, H. Brune, S. Rusponi and M. Fonin, *Nano Lett.*, 2017, **17**, 7177–7182.
- 9 M. Mannini, L. Sorace, L. Gorini, F. M. Piras, A. Caneschi, A. Magnani, S. Menichetti and D. Gatteschi, *Langmuir*, 2007, **23**, 2389–97.
- 10 L. Gorini, M. Fabrizioli, M. Mannini, L. Sorace and A. Yakovenko, *Inorg. Chim. Acta*, 2008, **361**, 4089–4093.
- 11 M. Mannini, P. Messina, L. Sorace, L. Gorini, M. Fabrizioli, A. Caneschi, Y. Manassen, P. Sigalotti, P. Pittana and D. Gatteschi, *Inorg. Chim. Acta*, 2007, **360**, 3837–3842.
- 12 M. Mannini, D. Rovai, L. Sorace, A. Perl, B. J. Ravoo, D. N. Reinhoudt, A. Caneschi and B. Jan, *Inorg. Chim. Acta*, 2008, **361**, 3525–3528.
- 13 J. L. Gallani, J. Le Moigne, L. Oswald, M. Bernard and P. Turek, *Langmuir*, 2001, **17**, 1104–1109.
- 14 P. Wautelet, J. Le Moigne, V. Videva, P. Turek and J. Le Moigne, *J. Org. Chem.*, 2003, **68**, 8025–36.
- 15 M. Tamura, Y. Nakazawa, D. Shiomi, K. Nozawa, Y. Hosokoshi, M. Ishikawa, M. Takahashi and M. Kinoshita, *Chem. Phys. Lett.*, 1991, **186**, 401–404.
- 16 J. Caro, J. Fraxedas, O. Jürgens, J. Santiso, C. Rovira, J. Veciana and A. Figueras, *Adv. Mater.*, 1998, **10**, 608–610.
- 17 R. Kakavandi, S.-A. Savu, A. Caneschi, T. Chassé and M. B. Casu, *Chem. Commun. (Camb.)*, 2013, 10103–10105.
- 18 S. Abb, S.-A. Savu, A. Caneschi, T. Chassé and M. B. Casu, *ACS Appl. Mater. Interf.*, 2013, **5**, 13006–13011.
- 19 J. Choi, H. Lee, K. Kim, B. Kim and S. Kim, *J. Phys. Chem.*

- Lett.*, 2010, **1**, 505–509.
- 20 H. Lee, S. Yang, J. Choi, Y. Park and S. Kim, *J. Phys. Chem. C*, 2011, **115**, 18736–18739.
- 21 A. Robin, L. Marnell, J. Bjork, M. S. Dyer, P. S. Bermudez, S. Haq, S. D. Barrett, M. Persson, A. Minoia, R. Lazzaroni and R. Raval, *J. Phys. Chem. C*, 2009, **113**, 13223–13230.
- 22 T. Junghoefer, E. M. Nowik-Boltyk, J. A. De Sousa, E. Giangrisostomi, R. Ovsyannikov, T. Chassé, J. Veciana, M. Mas-Torrent, C. Rovira, N. Crivillers and M. B. Casu, *Chem. Sci.*, 2020, **11**, 9162–9172.
- 23 F. Bonosi, G. Gabrielli, G. Martini and M. F. Ottaviani, *Langmuir*, 1989, **5**, 1037–1043.
- 24 J. M. Bennett, O. Warschkow and N. A. Marks, *J. Phys. Chem. C*, 2009, **113**, 1020–1027.
- 25 A. Caneschi, F. Ferraro, D. Gatteschi, A. le Lirzin and E. Rentschler, *Inorg. Chim. Acta*, 1995, **235**, 159–164.
- 26 K. Bernot, L. Bogani, A. Caneschi, D. Gatteschi and R. Sessoli, *J. Am. Chem. Soc.* 2006, **128**, 24, 7947–7956.
- 27 L. Bogani, C. Sangregorio, R. Sessoli and D. Gatteschi, *Angew. Chem. Int. Ed. Engl.*, 2005, **44**, 5817–21.
- 28 R. Sessoli, M.-E. Boulon, A. Caneschi, M. Mannini, L. Poggini, F. Wilhelm and A. Rogalev, *Nat. Phys.*, 2014, **11**, 69–74.
- 29 A. Collauto, M. Mannini, L. Sorace, A. Barbon, M. Brustolon and D. Gatteschi, *J. Mater. Chem.*, 2012, **22**, 22272.
- 30 M. Affronte and F. Troiani, in *Molecular Magnets: Physics and Applications*, eds. J. Bartolomé, F. Luis and J. F. Fernández, Springer Berlin Heidelberg, 2014, pp. 249–273.
- 31 M. Slota, A. Keerthi, W. K. Myers, E. Tret'yakov, M. Baumgarten, A. Ardavan, H. Sadeghi, C. J. Lambert, A. Narita, K. Müllen and L. Bogani, *Nature*, 2018, **561**, 691–695.
- 32 F. Ciccullo, A. Calzolari, K. Bader, P. Neugebauer, N. M. Gallagher, A. Rajca, J. Van Slageren and M. B. Casu, *ACS Appl. Mater. Interf.*, 2019, **11**, 1571–1578.
- 33 H. Atsumi, K. Maekawa, S. Nakazawa, D. Shiomi, K. Sato, M. Kitagawa, T. Takui and K. Nakatani, *Chem. - A Eur. J.*, 2012, **18**, 178–183.
- 34 L. Poggini, G. Cucinotta, A.-M. M. Pradipto, M. Scarrozza, P. Barone, A. Caneschi, P. Graziosi, M. Calbucci, R. Cecchini, V. A. Dediu, S. Picozzi, M. Mannini and R. Sessoli, *Adv. Mater. Interf.*, 2016, **3**, 1500855.
- 35 R. Frisenda, R. Gaudenzi, C. Franco, M. Mas-Torrent, C. Rovira, J. Veciana, I. Alcon, S. T. Bromley, E. Burzuri and H. S. J. Van Der Zant, *Nano Lett.*, 2015, **15**, 3109–3114.
- 36 F. Lombardi, A. Lodi, J. Ma, J. Liu, M. Slota, A. Narita, W. K. Myers, K. Müllen, X. Feng and L. Bogani, *Science*, 2019, **366**, 1107–1110.
- 37 L. Poggini, G. Cucinotta, L. Sorace, A. Caneschi, D. Gatteschi, R. Sessoli and M. Mannini, *Rend. Lincei. Sci. Fis. e Nat.*, 2018, **29**, 623–630.
- 38 M. H. Dishner, M. M. Ivey, S. Gorer, J. C. Hemminger and F. J. Feher, *J. Vac. Sci. Technol. A Vacuum, Surfaces, Film.*, 1998, **16**, 3295.
- 39 Y. Shirai, L. Cheng, B. Chen and J. M. Tour, *J. Am. Chem. Soc.*, 2006, **128**, 13479–89.
- 40 B. Genorio, T. He, A. Meden and S. Polanc, *Langmuir*, 2008, **24**, 11523–11532.
- 41 J. Vickerman and D. Briggs, *ToF-SIMS: Materials Analysis by Mass Spectrometry 2nd Edition*, IM Publications, 2013.
- 42 C. O'Dwyer, G. Gay, B. Viaris de Lesegno and J. Weiner, *Langmuir*, 2004, **20**, 8172–8182.
- 43 D. A. Chernova and A. K. Vorobiev, *J. Polym. Sci. Part B Polym. Phys.*, 2009, **47**, 107–120.
- 44 S. Stoll and A. Schweiger, *J. Magn. Reson.*, 2003, **163**, 248–256.
- 45 A. Bencini, G. Rajaraman, F. Totti and M. Tusa, *Superlattices Microstruct.*, 2009, **46**, 4–9.
- 46 G. Rajaraman, A. Caneschi, D. Gatteschi and F. Totti, *J. Mater. Chem.*, 2010, **20**, 10747–10754.
- 47 M. R. Ajayakumar, I. Alcón, S. T. Bromley, J. Veciana, C. Rovira and M. Mas-Torrent, *RSC Adv.*, 2017, **7**, 20076–20083.
- 48 V. Romanov, I. Bagryanskaya, D. Gorbunov, N. Gritsan, E. Zaytseva, D. Luneau and E. Tret'yakov, *Crystals*, 2018, **8**, 334.
- 49 Y. Zhang, S. Kahle, T. Herden, C. Stroh, M. Mayor, U. Schlickum, M. Ternes, P. Wahl and K. Kern, *Nat. Commun.*, 2013, **4**, 2110.
- 50 G. Rajaraman, A. Caneschi, D. Gatteschi and F. Totti, *Phys. Chem. Chem. Phys.*, 2011, **3**, 3886–95.
- 51 M. Jaccob, G. Rajaraman and F. Totti, *Theor. Chem. Acc.*, 2012, **131**, 1150.
- 52 H. Prüser, P. E. Dargel, M. Bouhassoune, R. G. Ulbrich, T. Pruschke, S. Lounis and M. Wenderoth, *Nat. Commun.*, 2014, **5**, 5417.
- 53 P. G. Barkley, J. P. Hornak and J. H. Freed, *J. Chem. Phys.*, 1986, **84**, 1886–1900.
- 54 Z. Zhang, A. Berg, H. Levanon, R. W. Fessenden and D. Meisel, *J. Am. Chem. Soc.*, 2003, **125**, 7959–7963.
- 55 V. Lloveras, E. Badetti, J. Veciana and J. Vidal-Gancedo, *Nanoscale*, 2016, **8**, 5049–5058.
- 56 V. Chechik, *J. Am. Chem. Soc.*, 2004, **126**, 7780–1.
- 57 S. S. Eaton and G. R. Eaton, in *Biological Magnetic Resonance* 2002, vol. 19, Springer, 29–154.